LASER INTERFEROMETER GRAVITATIONAL WAVE OBSERVATORY

LIGO Laboratory / LIGO Scientific Collaboration

LIGO-T040156-00-D *LIGO* August 6th 2004

Study of the Ouput Mode Cleaner Prototype using the Phasecamera

Joseph Betzwieser, Keita Kawabe and Luca Matone

Distribution of this document:

This is an internal working note
of the LIGO Project.

California Institute of Technology
LIGO Project – MS 18-34
1200 E. California Blvd.
Pasadena, CA 91125
Phone (626) 395-2129
Fax (626) 304-9834
E-mail: info@ligo.caltech.edu

Massachusetts Institute of Technology
LIGO Project – NW17-161
175 Albany St
Cambridge, MA 02139
Phone (617) 253-4824
Fax (617) 253-7014
E-mail: info@ligo.mit.edu

LIGO Hanford Observatory
P.O. Box 1970
Mail Stop S9-02
Richland WA 99352
Phone 509-372-8106
Fax 509-372-8137

LIGO Livingston Observatory
P.O. Box 940
Livingston, LA 70754
Phone 225-686-3100
Fax 225-686-7189

http://www.ligo.caltech.edu/

1 Introduction

This paper presents results of the phasecamera and how it was used to analyze the operation of the GEO Output Mode Cleaner on the LIGO Hanford 4km interferometer. We used the phasecamera, which spatially scans and demodulates incoming light to produce a spatial phase map of the beatings between the carrier and sidebands, to investigate the light input to and transmitted by the Output Mode Cleaner. We compared the data to our theoretical models of the Output Mode Cleaner.

2 Experimental Setup

2.1 Output Mode Cleaner

The Output Mode Cleaner (OMC) was placed on the Anti-Symmetric (AS) port of the Hanford 4k Interferometer. The OMC is a simple triangular cavity with a PZT attached to one mirror for length control. It was designed to pass the TEM00 carrier and sidebands through the same resonance, while rejecting all the higher order modes. The cavity was held on resonance by maximizing the light on transmission and applying a small dither signal to the OMC length at 40khz, and using a lock-in amplifier to servo off this error signal. A few useful parameters of the OMC are shown later in table 1. For a complete description of the OMC go to LIGO document T040018.

2.2 Incoming Light

We have modeled and taken data for the OMC in the two simplifying cases of straight shot of the laser off an ITM into the AS port and of the interferometer being held in a bright Michelson lock. In these cases we assume that the modal content of the incoming carrier and sideband is essentially the same. However, a beam scan of the light on the table showed the light to be astigmatic, complicating the situation[1]. The light had a first beam waist of 137μm along an axis rotated 25 degrees counterclockwise relative to the OMC horizontal axis. The second beam waist of 107μm located 6.6cm after the first waist was along an axis rotated 25 degrees relative to the OMC vertical axis[2]. Initially, the OMC was mode matched to only the horizontal waist, treating that as the only waist. However, during the testing process it was moved such that the transmission through the OMC was maximized. All data present here is from this later situation.

2.3 Phasecamera

The phasecamera is the combination of a position scanning galvanometer and a New Focus 1811A RF photodiode. The galvanometer moves the incoming light in a spiral pattern on the photodiode at a rate of about one full scan every half second. The two output channels of the photodiode, DC power and RF power, are then sampled at a rate of up to 4000 points per full scan. The RF sampled points are then demodulated and passed to a computer, along with the position readback of the galvanometer. In this case the demodulation frequency used is 25 Mhz, so as to look at the beat

between the carrier and sideband of the incoming light. This data then can be used to plot the spatial profile of the DC power and the I and Q phases of the demodulated light. For more information, go to LIGO Document P030069-00-R.

In this experiment a 50/50 beamsplitter was placed on transmission of the OMC, redirecting half of the transmitted light to the phasecamera. On the path to the phasecamera, two lenses were placed so as to focus the light to the proper size to be scanned. This meant the phasecamera photodiode was approximately 0.45m from a waist size of 150μm, resulting in a Gouy phase of nearly $\pi/2$ radians.

3 Theory and Modeling

3.1 The Astigmatic Beam

The Hermite Gaussian basis provides a complete set of solutions for the fields which can propagate inside or outside of the cavity. These solutions, which have been normalized for power, have the form

$$\Psi_{mn} = \sqrt{\frac{2}{2^{(m+n)} m!n!p}} \frac{1}{w(z)} H_m\left(\frac{\sqrt{2}x}{w(z)}\right) H_n\left(\frac{\sqrt{2}y}{w(z)}\right) e^{-\frac{(x^2+y^2)}{w(z)^2}} e^{-\frac{ik(x^2+y^2)}{2R(z)}} e^{ikz} e^{i(m+n+1)\tan^{-1}\left(\frac{zl}{p w_0^2}\right)} \quad (1)$$

where m and n are the TEM mode numbers, x and y are the distances from the center of the beam perpendicular to the direction of propagation, z is the distance from the waist in the direction of propagation, $w(z)$ is the radius of the beam at z, w_0 is the radius at the waist, $R(z)$ is the radius of curvature of the beam front at z, λ is the wavelength of light, k is the wave number ($2\pi/\lambda$), and H_m is the Hermite polynomial of order m.

This can be generalized for the incoming light by breaking up the symmetry between the x and y axes and allowing them to have different waists and waist positions. In the case of a bright Michelson lock and also a straight shot of the laser light off an ITM, the light should be a pure TEM00, distorted only by the astigmatism. Thus, the incoming light can be written as

$$\Psi_{astigmatic}(x',y',z') = \sqrt{\frac{2}{2^{(m+n)} m!n!p}} \sqrt{\frac{1}{w_x(z_x)}} \sqrt{\frac{1}{w_y(z_y)}} H_m\left(\frac{\sqrt{2}x}{w_x(z_x)}\right) H_n\left(\frac{\sqrt{2}x}{w_y(z_y)}\right) \times$$
$$\times e^{-\left(\frac{x}{w_x(z_x)}\right)^2 - \left(\frac{y}{w_y(z_y)}\right)^2} e^{ik\left(\frac{z_x+z_y}{2}\right)} e^{i\left(m+\frac{1}{2}\right)\tan^{-1}\left(\frac{z_x l}{p w_{0x}(z_x)^2}\right)} e^{i\left(n+\frac{1}{2}\right)\tan^{-1}\left(\frac{z_y l}{p w_{0y}(z_y)^2}\right)} \quad (2)$$

3.2 The OMC Basis

The OMC cavity imposes several boundary conditions on the general Hermite Gaussian solutions of equation 1. First, for resonance to occur, after each full round trip the phase and amplitude must match. Second, at the curved back mirror the wave front of the beam must match that of the cavity (neglecting the small incidence angle). Also note that because of symmetry the waist of the beam inside the cavity must occur midway between the two flat mirrors and opposite the curved back mirror. These conditions imply the following

$$w_0^4 = \left(\frac{l}{p}\right)^2 L(R_0 - L)$$
$$\frac{n}{n_0} = (q+1) + \frac{1}{p}(m+n+1)\cos^{-1}\left(\sqrt{1-\frac{L}{R_0}}\right) + \frac{1}{2}Mod_2(m) \quad (3)$$

where L is half the round trip length, R_0 is the radius of curvature of the back mirror and ν_0 is the free spectral range (FSR). The FSR is equal to $c/2L$, where c is the speed of light, and is simply the distance in frequency space between successive transmission peaks. These transmission peaks are numbered by the q parameter, since q+1 is the number of half wavelengths inside the cavity. The modulo base 2 term comes from the fact that the cavity is triangular, and that for odd mode numbers in the direction parallel to the mode cleaner plane there is an additional π phase shift in the round trip. Table 1 provides the values for these and several other related parameters of the OMC.

Table 1: OMC parameters

Cavity Finesse	~30[3]
Half of Round Trip Path (L)	50.75mm
End Mirror Radius of Curvature (R_0)	75mm
Free Spectral Range (ν_0)	2.95 GHz
Beam waist inside the OMC (w_0)	109μm
Wavelength of Carrier light (λ)	1064nm

The important part of equation 3 is that for a given frequency of light, each sum of m plus n needs a different length of cavity to resonate. This means the OMC will decompose the incoming light into the Hermite Gaussian basis and only let those modes whose m + n satisfy equation 3 to pass, generally the carrier TEM00 mode. All others will be reflected back from the OMC. However, because the mirrors of the OMC do not have 100 percent reflectivity, the range of frequencies which can pass are broadened, allowing most of the sideband TEM00 modes to pass. This can be seen by looking at the transmitted light of the OMC, considering the reflection and transmission at each mirror. Assuming no losses in the cavity and no transmission on the end mirror, the complex amplitude of the transmitted light will be

$$\Psi_{transmitted} = \frac{t_1 t_2 \Psi_{incident}}{1 - r_1 r_2 e^{ij}} \quad (4)$$

where

$$j = 2kL - 2(m+n+1)\cos^{-1}\left(\sqrt{1-\frac{L}{R_0}}\right) - p\,Mod_2(m),$$

t_1 equals t_2 and represent the transmission of the mirros, r_1 equals r_2 and represent the reflectivity of the mirrors, and assuming $t^2 + r^2 = 1$. The *k* represents the wavenumber of the light and varies due to the 25MHz frequency difference between the carrier and sidebands, resulting in a different transmission ratio for the carrier and sidebands of the same mode.

3.3 Decomposing the Astigmatic Beam into the OMC basis

In light of equations 3 and 4, we need to decompose the general astigmatic beam (Eq. 2), into the Hermite Gaussian basis of the OMC (Eq. 1) in order to understand how it passes through. This was done in two ways, both of which resulted in the same decomposition. The first decomposition was done by taking the inner product between the astigmatic beam and a particular OMC mode, essentially the inner product between equations 1 and 2. This inner product,

$$\int_{-\infty}^{\infty} \Psi_{mn} \Psi^*_{astigmatic} = a_{mn} e^{iq_{mn}} \tag{5}$$

yields the amplitude and phase of the TEM_{mn} mode present in the beam.

The other method of decomposition started with creating a set of theoretical data with equation 2, with the amplitude of the astigmatic beam stored at a series of x and y coordinates. The following simple model was then fit to this artificial data set

$$a_{00} e^{iq_{00}} \Psi_{00} + a_{01} e^{iq_{01}} \Psi_{01} + a_{10} e^{iq_{10}} \Psi_{10} + a_{02} e^{iq_{02}} \Psi_{02} + a_{11} e^{iq_{11}} \Psi_{11} + a_{20} e^{iq_{20}} \Psi_{20}\,, \tag{6}$$

where Ψ_{mn} is the *mn* OMC mode. The amplitude and phase of each of the modes (defined by equation 1) is then left as a free parameter of the model. After fitting, we normalize the model by scaling so that the TEM00 mode has an amplitude of one and a phase of zero. This second method is very similar to the one used to analyze the phasecamera data. The results of the two decompositions were very close, providing a nice confirmation of the fitting method.

There are two additional decompositions which can provide insight, that of an astigmatic beam with the 25 degrees of rotation, where the two waist's axes are aligned with the OMC axes, and that of an astigmatic beam misaligned in vertical displacement coming into the OMC. In the first case, the TEM11 mode completely disappears, leaving only the expected TEM02 and TEM20 modes due to the mode mismatch[4]. In the second case a vertical displacement of one third the waist size of the OMC was somewhat arbitrarily chosen because of measurements indicating alignment drift of this size on short time scales.[5] This decomposition gives a feel for what deviations to expect between the OMC model and the phasecamera data. The differences are mostly on the order of 15 percent for modes that are present in the perfect alignment and the inclusion of several "misalignment" modes, such as the TEM01. Table 2 summarizes all of these decompositions.

Lastly, to calculate the astigmatic beam on transmission of the OMC, one simply needs to apply equation 4 to each mode for both the carrier and sidebands. Then add all the modes back together for the carrier or the sideband.

Table 2: Astigmatic Beam decompositions

Mode	Integration Method		Fit Method		Integration Method, Misaligned		Integration Method, Non-rotated	
	Amplitude	Phase In degrees	Amplitude	Phase In degrees	Amplitude	Phase In degrees	Amplitude	Phase In degrees
00	1	0	1	0	1	0	1	0
01	-	-	-	-	0.28	-155	-	-
10	-	-	-	-	.13	25	-	-
02	0.23	-57	0.24	-56	0.22	-43	0.28	-150
11	0.26	80	0.25	77	.23	87	-	-
20	0.21	31	0.22	26	0.22	32	0.47	39
03	-	-	-	-	0.11	153	-	-
12	-	-	-	-	0.12	-63	-	-
21	-	-	-	-	0.05	-172	-	-
30	-	-	-	-	0.05	57	-	-
04	0.07	-113	0.07	-113	0.06	-86	0.19	-136
13	0.11	23	0.11	21	0.09	43	-	-
22	0.02	176	0.01	177	0.003	-161	0.02	38
31	0.10	111	0.10	103	0.09	117	-	-
40	0.06	62	0.06	51	0.061	64	0.15	45
05	-	-	-	-	0.041	101	-	-
14	-	-	-	-	0.06	-120	-	-
23	-	-	-	-	0.02	46	-	-
32	-	-	-	-	0.04	-46	-	-
41	-	-	-	-	0.02	-181	-	-
50	-	-	-	-	0.02	88	-	-

3.4 Decomposition comparison to Bright Michelson OMC scans

One straightforward experimental test of the astigmatic decomposition is to tune the OMC's length such that modes other than the TEM00 become resonant and note the power of the transmitted light. In practice this is done by applying a slowly increasing voltage to the OMC's PZT to change

the length of the OMC while continuously recording the power of the light on transmission. By calculating the transverse mode spacing (TMS) from

$$TMS = \frac{1}{p}\arccos\left(\sqrt{(1 - L/R_0)}\right) \tag{7}$$

we can easily match peaks with sets of degenerate modes, since a TEM_{mn} mode will be shifted in frequency from the TEM00 mode by $(m+n)*TMS$ in units of free spectral range. For the OMC, the TMS is about 0.305[6]. To compare the astigmatic decomposition to data taken in this way during a bright Michelson lock, we need to apply the OMC response function (equation 4) to the mode amplitudes from table 2 while letting L vary, which lets us go through a free spectral range of resonant frequencies. Then we take the power in each mode, sum them all, and plot as a function of free spectral range. The final formula used is thus

$$A\left(a_{00}{}^2 \left|T_{00}^{carrier}(dL)\right|^2 + a_{01}{}^2 \left|T_{01}^{carrier}(dL)\right|^2 + ...\right) \tag{8}$$

where a_{mn} and θ_{mn} are amplitude and phase of mode *mn* from table 2, $T_{mn}(dL)$ is the response of the OMC for mode *mn* for a given length change *dL*, and *A* is an overall scale para meter. Note that we ignore the effects of the sidebands in this calculation since for the bright Michelson lock the DC power is dominated by the carrier. Figure 1 shows a plot of scan data taken during a bright Michelson lock that is overlaid with equation 8 as a function of dL. In addition, to produce numbers we can compare we fit the scan data to the simple model of

$$Power(dL) = \sum_{m,n}^{m+n=4} A_{mn} \left|T_{mn}^{carrier}(dL)\right|^2 \tag{9}$$

where $T_{mn}^{carrier}(dL)$ is the OMC response function and A_{mn} are the free parameters of the fit. A_{mn} are just the square of a_{mn}. Due to degeneracy between modes, we can't completely distinguish A_{mn} terms, but we can compare the sums of the degenerate modes. Table 3 provides a comparison of these sums from the model and the OMC scan, with all values normalized to a TEM00 transmission of 1. Both figure 1 and table 3 show a very strong correspondence between our model's prediction and the actual experimental result, especially when we consider that the model assumes perfect alignment and thus predicts no misalignment modes such as 10 and 01.

Table 3: Fit and Model of OMC scan

Degenerate Mode	Modes	Fit (Power in modes)	Model (Power in modes)	Misaligned Model (Power in modes)
1 even	01	0.1396	-	.0784
1 odd	10	-	-	.0169
2 even	20,02	0.1040	0.1004	.0968
2 odd	11	0.0633	0.0686	.0529
3 even	03,21	0.0240	-	.0146
3 odd	12,30	0.0232	-	.0169
4 even	04,22,40	0.0066	0.0080	.0073
4 odd	13,31	0.0214	0.0206	.0162
5 even	05,23,41	0.0128	-	.0025
5 odd	50,32,14	-	-	.0056

The break in the degeneracy between modes of the same m + n value is due to the triangular nature of the cavity and thus for odd mode numbers in the direction parallel to the mode cleaner plane there is an additional 0.5 FSR shift in resonance frequency.

Figure 1: Modal Decomposition – Black: Data, Blue: Model, Red: Fit

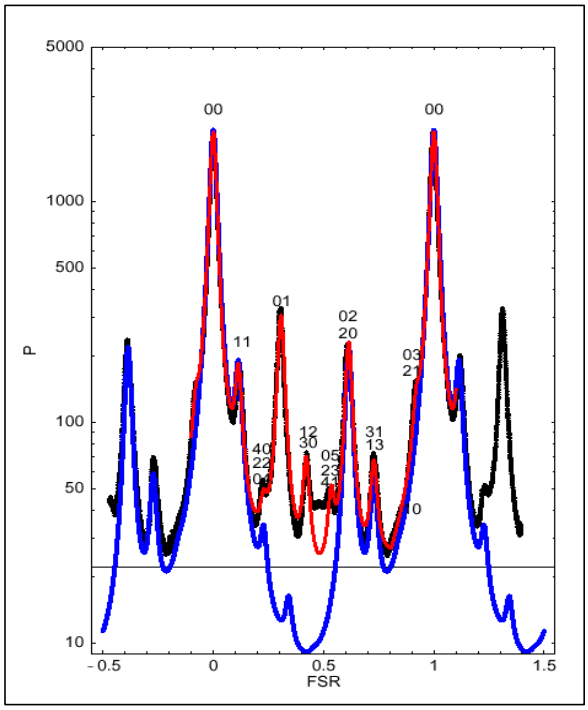

3.5 What the Phasecamera Should See

The phasecamera sees the strength of the beat between the carrier and the sidebands, by demodulating at 25Mhz. The sidebands are generated from the carrier via phase modulation of the form

$$E_0 e^{i(wt+\Gamma\sin(\Omega t))} \approx E_0\left[J_0(\Gamma)e^{iwt} + J_1(\Gamma)e^{i(w+\Omega)t} - J_1(\Gamma)e^{i(w-\Omega)t}\right] \tag{10}$$

where E_0 is the original carrier amplitude, ω is the angular frequency of the carrier, Ω is the frequency of the modulation, Γ is the modulation depth, and t is time. The approximation on the right of equation 10 is simply an expansion and then collection of terms into Bessel functions of 0^{th} and 1^{st} order. The first, second and third terms on the right are the carrier amplitude, the upper sideband amplitude, and the lower sideband amplitude respectively. Since the carrier and sidebands see the same surfaces for a bright Michelson lock or a direct reflection off an ITM, and the sideband generation should only produce a frequency and amplitude difference between the sideband and carrier, it is reasonable to assume that the modal content will be the same for both. In that case we can write the individual field amplitudes of the carrier and sidebands as

$$\begin{aligned}
A_{carrier} &= E_0 J_0(\Gamma)\left(a_{00}e^{iq_{00}}T_{00carrier}\Psi_{00} + a_{01}e^{iq_{01}}T_{01carrier}\Psi_{01} + \ldots\right)\\
A_{sb+} &= E_0 J_1(\Gamma)\left(a_{00}e^{iq_{00}}T_{00sb+}\Psi_{00} + a_{01}e^{iq_{01}}T_{01sb+}\Psi_{01} + \ldots\right)\\
A_{sb-} &= -E_0 J_1(\Gamma)\left(a_{00}e^{iq_{00}}T_{00sb-}\Psi_{00} + a_{01}e^{iq_{01}}T_{01sb-}\Psi_{01} + \ldots\right)
\end{aligned} \tag{11}$$

where $T_{00carrier}$ is the OMC response , obtained from $\frac{\Psi_{transmitted}}{\Psi_{incident}}$ from equation 4 for the appropriate mode, and the ψ_{mn} are from equation 1 with the Gouy phases fixed to match that of the experimental setup. The total field of the light can then be written as

$$A_{carrier}e^{iwt} + A_{sb+}e^{i(w+\Omega)t} + A_{sb-}e^{i(w-\Omega)t} \tag{12}$$

where ω is the angular frequency of the carrier and Ω is the sideband modulation angular frequency.

Demodulating the power in phase at angular frequency Ω yields the in phase (I phase), and 90 out of phase yields the quadrature phase (Q phase). These can be explicitly written as

$$\begin{aligned}
2\mathrm{Re}\left(A_{carrier}A_{sb+}^{*} + A_{carrier}^{*}A_{sb-}\right) &= Qphase\\
2\mathrm{Im}(A_{carrier}A_{sb+}^{*} + A_{carrier}^{*}A_{sb-}) &= Iphase
\end{aligned} \tag{13}$$

By replacing the amplitudes a_{mn} and phases θ_{mn} with the appropriate model values we can create an I or Q phase map which is directly comparable to the phasecamera phase maps. The phase map in figure 2 is created using the parameters from the integration method of astigmatic beam decomposition listed in table 2, with an overall demodulation phase rotation such that all the higher order mode "junk" is in one phase but not the other.

Figure 2: Phase map generated from OMC model, with parameters from table 2

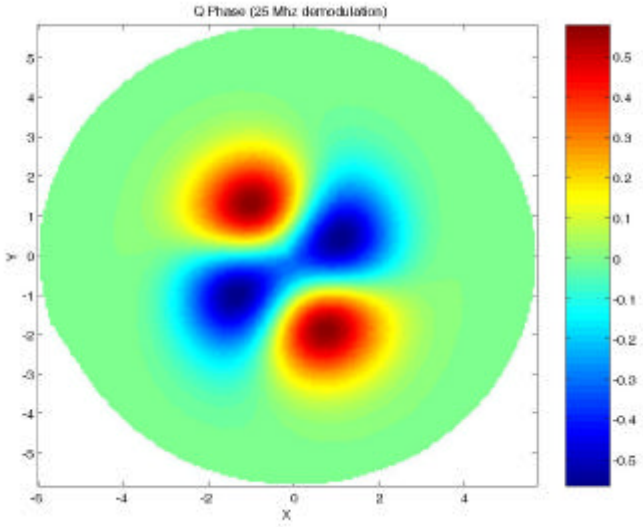

4 Phasecamera Measurements and Comparisons

4.1 Phasecamera Data

The following images were taken by the phasecamera in two different states. The first was when the OMC was locked with maximum light transmission while the interferometer was held on a bright Michelson fringe. The second was when the interferometer was misaligned except for ITMY and the BS, resulting in a straight shot of light into the antisymmetric port. The images are reproducible for a given status of the interferometer.

Figure 3: Bright Michelson Lock on transmission of the OMC

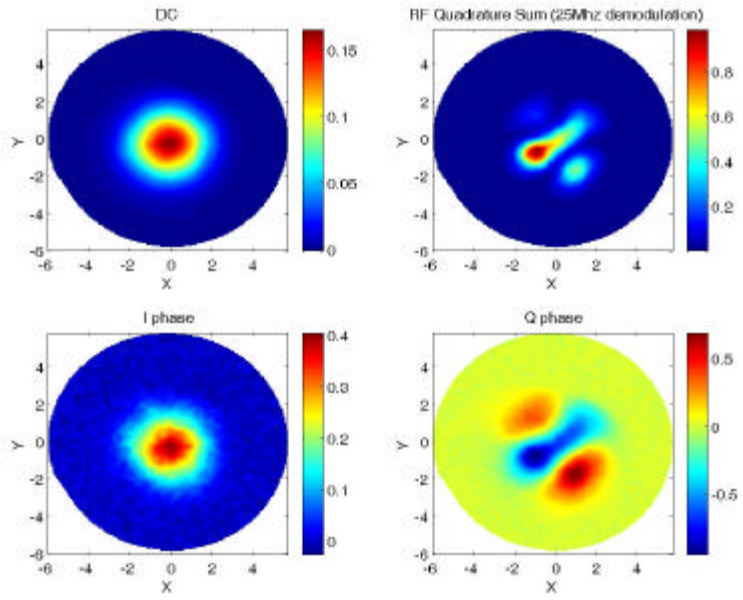

Figure 4: Straight Shot off ITMY on transmission of OMC

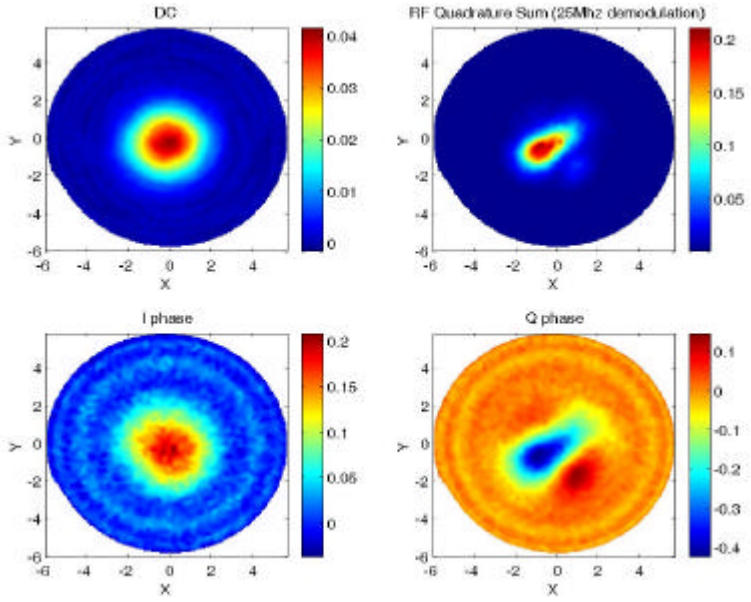

The DC power images show fairly clean TEM00 modes, indicating the OMC is in fact transmitting mostly the mode we want. The factor of 4 drop in DC power intensity from the bright Michelson to the straight shot is due to the loss of 50% of the light at the beam splitter because of the ITMX misalignment. The I and Q phases have been rotated to match the same overall phase rotation chosen for the model, so that one phase is expected to be flat and the other will contain the higher order modes transmitted. The fact that we see a clear TEM00 mode in one phase instead of a flat plane implies some amplitude modulation of the carrier and sidebands is being produced by or passing through the OMC. The TEM11 mode image in the Q phase is reassuring, as it looks similar to the model prediction from figure 2.

To determine if the TEM00 mode present in the I phase is due to the OMC or present on the light before reaching the OMC, we look at phasecamera images when the OMC was removed. Figure 5 and 6 show the bright Michelson lock and an ITM straight shot without the OMC in the path. In the bright Michelson case the amplitude modulation can be fully explained as being on the incoming light, since the ratio of the DC power to the I phase power is roughly the same or less for the OMC present and not present cases as shown in Table 4. However, for the case of the straight shot off an ITM, the amplitude modulation seems to be greater after the OMC. This could be explained by the OMC simply not being on resonance and thus generating excess amplitude modulation.

Figure 5: Bright Michelson directly to Phasecamera

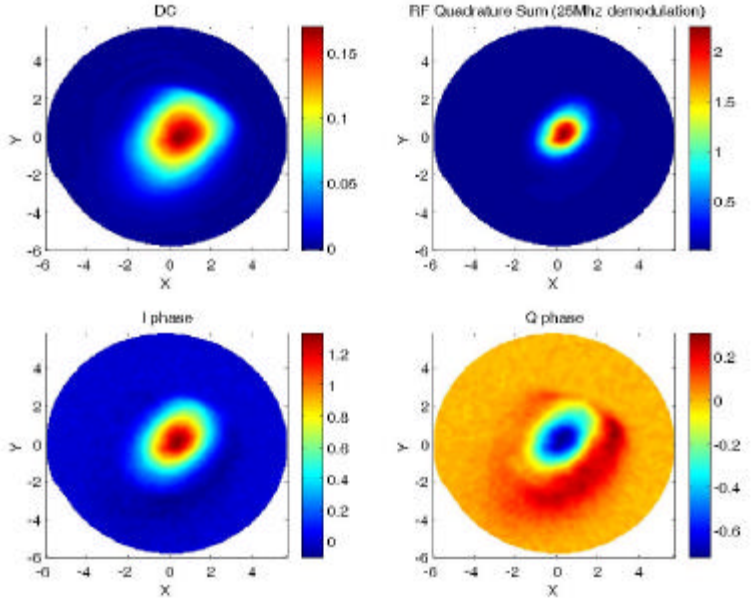

Figure 6: Straight Shot off ITMX directly to Phasecamera

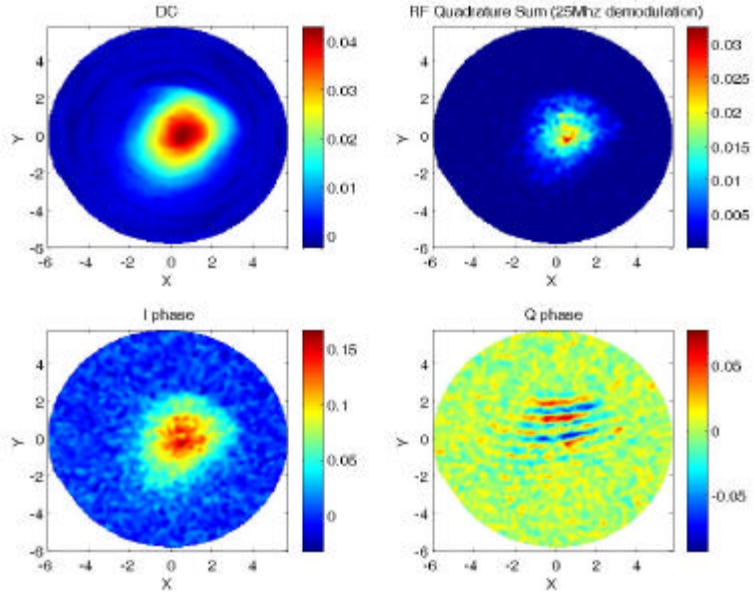

Table 4: Amplitude Modulation comparisons

	Data Set 1 Ratio of Iphase/DC	Data Set 2 Ratio of Iphase/DC	Data Set 3 Ratio of Iphase/DC
Bright Michelson With OMC	2.28	2.48	2.45
Bright Michelson Without OMC	3.7	3.68	3.74
Straight Shot With OMC	7.03	3.9	4.97
Straight Shot Without OMC	3.12	3.18	3.2

4.2 Phasecamera and Model comparison

To directly compare the models, we first need to set certain scale parameters. The easiest method of getting these scale parameters is to fit the DC power data to $A\Psi_{00}\Psi^{*}_{00}(x+x_{offset}, y+y_{offset}, w)$, letting the overall amplitude A, the center position offsets x_{offset} and y_{offset}, and w the waist size vary as free parameters. Fixing the offsets and waist size in our model first makes the final stage of fitting to the model much easier. We then make a nonlinear fit of equation 13 to the data, treating $E_0^2 J_0(\Gamma)J_1(\Gamma)$ as a single amplitude free parameter A in addition to the a_{00} and q_{00} free parameters. We use the values from table 2 as our initial guesses, and restrict the parameter space to about ±20 percent of those values. To determine the quality of the fit, we first determine the noise in the data. By subtracting phasecamera images from one another, and taking the standard deviation of the resulting difference values gives us our σ. We then use this to calculate our χ^2 (normalized) merit functions with values of about between 0.8 to 3.9, depending on how noisy a particular image is and whether it was bright Michelson or straight shot. However, the residuals show some distinct structure excess, perhaps some TEM00 mixed with TEM20 in the case of the straight shot fits. The following two fits of the Q phase, one for the bright Michelson and one for the straight shot are typical of the sets.

Figure 7: Q phase fit of Bright Michelson Data

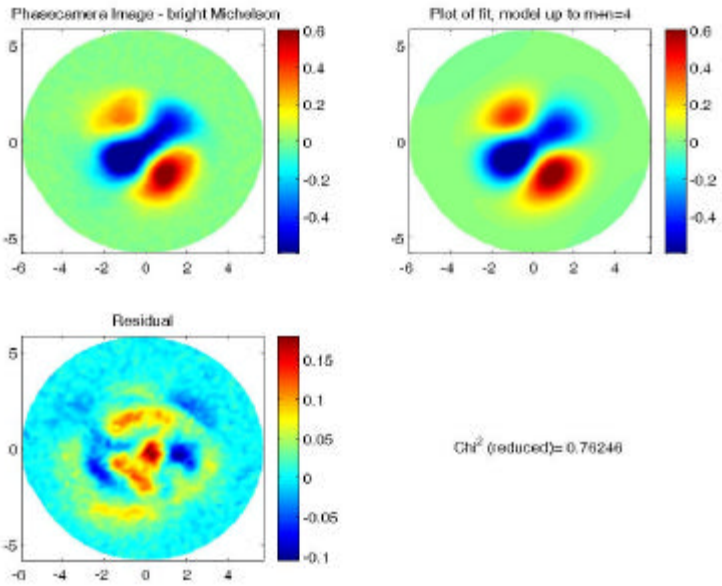

Figure 8: Q phase fit of Straight Shot off ITM data

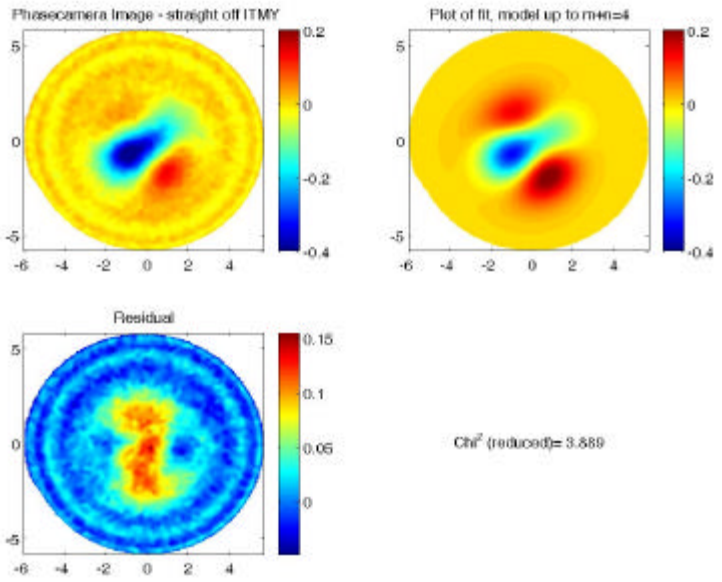

Table 5 gives the parameter values for the two sets of measurements, along with the model values from table 2, normalized to a TEM00 amplitude of 1 and a phase of 0. This comparison provides several insights. The large TEM01 mode implies a significant misalignment on the vertical axis between the incoming light and the OMC, on the order of the waist size or the divergence angle of the light at the OMC[7]. The TEM02,TEM11, and TEM20 modes are consistent with being produced solely by the astigmatic nature of the light. Ignoring the effects of a simple misalignment, the fact that the model matches the data well implies the OMC is doing what it is

expected to be doing. We're getting large amounts of higher order modes on transmission of the OMC mostly due to the known astigmatism, and that other additional problems or effects are unnecessary to explain the OMC output.

Table 5: Model and Fit comparisons for both the Bright Michelson and Straight Shot

Mode	Model		Misaligned Model		Bright Mich		Straight Shot	
	Amplitude	Phase In Degrees	Amplitude	Phase In Degrees	Amplitude	Phase In Degrees	Amplitude	Phase In Degrees
χ^2 (normalized)	-	-	-	-	0.802	-	3.889	-
A	-	-	-	-	258	-	99	-
00	1	0	1	0	1	0	1	0
01	-	-	0.28	-155	0.43	71	0.50	62
10	-	-	.13	25	0.044	-15	0.066	2
02	0.23	-57	0.22	-43	0.30	-44	0.30	-72
11	0.26	80	.23	87	0.256	100	0.20	100
20	0.21	31	0.22	32	0.27	11	.27	11
03	-	-	0.11	153	0.023	12	0.03	12
12	-	-	0.12	-63	0.09	-70	0.04	62
21	-	-	0.05	-172	0.06	-17	0.06	-38
30	-	-	0.05	57	0.080	59	0.12	34
04	0.07	-113	0.06	-86	0.02	-90	0.02	-90
13	0.11	23	0.09	43	0.127	129	0.11	175
22	0.02	176	0.003	-161	0.03	191	0.03	191
31	0.10	111	0.09	117	0.10	131	0.08	91
40	0.06	62	0.061	64	0.04	82	.04	82

5 Conclusions

This paper has demonstrated agreement between a theoretical model of the OMC and the data produced by the phasecamera. It shows that our understanding of what the OMC is doing is correct, that most of the higher order mode transmission is due to the astigmatic nature of the light. At the time of this writing, we are in the process of finishing the phasecamera installation by the final alignment of a reference laser for the phasecamera, which will allow us to optically

heterodyne the incoming light and demodulate each sideband and the carrier individually, providing more detailed information and making modal fitting significantly easier. With maps of the incoming carrier and sidebands, we should be able to make sense of the much more complicated structure of the fully locked interferometer.

6 References

1. Luca and Joe, Joe's Elog on Wensday April 14th,2004
2. Luca, Hiro and Joe, Luca's Elog on Thursday July 15th, 2004
3. Keita's Elog on Tuesday, June 15th 2004
4. Luca's Elog on Thursday June 17th, 2004
5. Luca and Joe, Joe's Elog on Monday May 17th, 2004
6. Keita's Elog on Wednesday May 26th, 2004
7. D. Anderson, "Alignment of resonant optical cavities", Appl. Opt. 23,2945 (1984).
8. K. Goda, D. Ottaway, B. Connelly, R. Adhikari and N. Mavalvala, "Frequency Resolving Spatiotemporal Wavefront Sensor", LIGO-P030069-00-R
9. H. Kogelnik and T. Li, "Lasers Beams and Resonantors", Appl. Opt. 5, 1550 (1966).
10. Keita's Elog on Monday June 28th, 2004
11. Keita, Luca and Joe, Keita's Elog on Friday June 11th, 2004